Constraining the relationships between aerosol height, aerosol optical depth and total column trace gas measurements using remote sensing and models

Shuo Wang[1], Jason Blake Cohen[1, 2, *], Chuyong Lin[1], Weizhi Deng[1]

[1]School of Atmospheric Sciences, Sun Yat-Sen University, Guangzhou, 519000, China
[2]Southern Marine Science and Engineering Guangdong Laboratory (Zhuhai)

Correspondence to: Jason Blake Cohen (jasonbc@alum.mit.edu)

Abstract. Proper quantification of the aerosol vertical height is essential to constrain the atmospheric distribution and lifetime of aerosols, as well as their impact on the environment. We use globally distributed, daily averaged measurements of aerosol stereo heights of fire aerosols from MISR to understand the aerosol distribution. We also connect these results with a simple plume rise model and a new multi-linear regression model approach based on daily measurements of NO_2 from OMI and CO from MOPITT to understand and model the global aerosol vertical height profile over biomass burning regions. First, plumes associated with the local dry-burning season at mid to high latitudes frequently have a significant fraction lofted into the free troposphere, and in some cases even the stratosphere. Second, plumes mainly associated with less polluted regions in developing countries and heavily forested areas tend to stay closer to the ground, although they are not always uniformly distributed throughout the boundary layer. Third, plumes associated with more serious loadings of pollution (such as in Africa, Southeast Asia and Northeast China) tend to have a significant amount of smoke transported uniformly through the planetary boundary layer and up to around 3 km. Fourth, the regression model approach yields a better ability to reproduce the measured heights as compared to the plume rise model approach. This improvement is based on a removal of the negative bias observed from the plume model approach, as well as a better ability to work under more heavily polluted conditions. However, over many regions, both approaches fail, requiring deeper work to understand the physical, chemical, and dynamical reasons underlying the failure over these regions.

1 Introduction

Over the past few decades, there has been an increasing amount of research into the spatial and temporal distribution of atmospheric aerosols (Achtemeier et al., 2011; Cohen et al., 2017; Cohen et al., 2018). This has been in part because of the impacts that aerosols have on clouds, radiation, the atmospheric energy balance and climate, human health, and ecosystems, among other aspects (Val Martin et al., 2012; Nelson et al., 2013; Cohen,2014). However, there has not been a significant amount of research work done in terms of understanding the vertical distribution of aerosols in the atmosphere(Cohen et al., 2018), although such knowledge is essential to constrain their impacts the atmospheric energy budget (Kim et al., 2008; Mims

30   et al., 2010), circulation, clouds and precipitation(Cohen et al., 2011; Tosca et al., 2011; Singh et al., 2018), and ultimate

tropospheric distribution (Leung et al., 2007; Winker et al., 2013).

The vertical distribution of aerosols is known to be more complex in regions where there are multiple significant sources

with different vertical lofting properties (Kahn et al., 2007; Petrenko et al., 2012; Chew et al., 2013). While on one hand urban

sources are emitted at relatively low heat are known to remain in the boundary layer (Guo et al., 2016), on the other, biomass

35   burning sources are emitted at high temperature and frequently are emitted high in the atmosphere (Ichoku et al., 2008; Field et

al., 2009; Freeborn et al., 2014). Furthermore, there are other forcing mechanisms, such as deep convection (Petersen and

Rutledge 2001; Turquety et al., 2007), volcanos (Singh et al., 2018; Vernon et al., 2018), mountain slope winds (Cohen et al.,

2017), and other dynamical forcings (Cohen et al., 2011; Tosca et al., 2011) which also have a significant effect on the vertical

distribution of aerosols over specific spatial and temporal scales. The vertical distribution of aerosols has a direct impact on

40   their lifetime and hence atmospheric loading, with aerosols lofted above the boundary layer having a significantly larger

impact the atmosphere than those emitted into the boundary layer (Nelson et al., 2013; Paugam et al., 2016). Therefore,

understanding the vertical distribution over the source regions (Nelson et al., 2013) of aerosols and how this may change over

time is absolutely critical for our being able to better constrain the environmental and atmospheric impacts.

Currently, aerosol data comes from different measurements made from the surface, balloons, aircraft, and satellites, with

45   varying degrees of accuracy (Husar et al., 1997, Jost et al., 2004, Rogers et al., 2011) used in-situ measurements to observe the

plume from North American fires emitted at a surface temperature above 380K, and found that carbon monoxide and tiny

particles were detected in the stratosphere at an altitude of 15.8 km. Kahn et al. (2007) found using MISR measurements that

5% to 18% of smoke plumes reached the free troposphere over Alaska and the Yukon Territories in 2004.Val Martin et al.

(2018) introduced the idea of possibly using CALIPSO LIDAR as a measurement technique, since it is more sensitive to

50   dispersed vertical aerosols away from fire points than MISR satellites, and therefore could capture the overall smoke cloud

better. Val Martin et al. (2018) used MISR data with pixel-weighted and AOD-weighted statistics to estimate the impact of fire

severity of on fire height and found that in almost all areas, there is a significant amount of aerosols above 2 km. Cohen et al.

(2018) produced the first comprehensive study using CALIPSO LIDAR data anywhere in the world, and found that throughout

the 2006 biomass burning season in Southeast Asia that 51% to 91% of smoke from fires was ultimately found to reside in the

55   free troposphere. This is consistent with earlier theory by which show that when a plume is injected into the free troposphere,

it tends to accumulate in a relatively stable layer (Val Martin et al., 2010; Kahn et al., 2007).

The present generation of models have not been found to reproduce the vertical distribution of aerosols very well (Ichoku

and Ellison, 2014; Cohen et al., 2018). Most of the previous approaches to simulate convection induced by a fire or other

surface heat sources have been performed with simplified models (Briggs, 1965; Trentmann et al., 2006). There have been

60   multiple studies using global and regional chemical transport models (CTMs) with such simple plume models built in to try to

understand the impact of fire emissions on air quality and atmospheric composition (Pfister et al., 2008; Turquety et al., 2007;

Spracklen et al., 2009; Ichoku and Ellison 2014). There have also been other attempts to simulate the impacts of different

vertical distributions based on higher-resolution wind patterns profiles, done on a region-by-region basis (Cohen and Prinn,

2011; Cohen and Wang, 2014). More recently, people have attempted to use Lagrangian models such as Dewitt and Gasore

65   (2019) and Vernon et al. (2018), to understand how knowledge of air mass flows could better contribute to the understanding

of different vertical regions having material from biomass burning plumes found far upwind. Val Martin et al. (2012) used a

1-D plume rise model to study plume heights over North America, which demonstrated dynamical heat flux and atmospheric

stability structure affect plume rise. Cohen et al. (2018) also adapted a plume rise model and found that significant

enhancements were required to the measured Fire Radiative Power (FRP) values in order to match the mean values of

70   measured heights, although the upper and lower quartiles were not able to be successfully reproduced. At present, there is no

known modelling work that can accurately and consistently reproduce this significant atmospheric loading found throughout

different regions of the world in the upper boundary layer and free troposphere.

Biomass combustion is a major source of trace gases and aerosols in the atmosphere as well as having a significant impact

on tropospheric ozone formation. The vast majority of biomass burning is a man-made activity (Kauffman et al., 2003;

75   Achtemeier et al., 2011; Paugam et al., 2016). In particular, this activity has been shown to have a strong annual cycle (Cohen

et al., 2017; Labonne et al., 2007; Tsigaridis et al., 2014). The process of burning releases heat, increasing the local temperature

of the surrounding air, resulting in a change in buoyancy and an ensuing updraft above the heat-producing area. Based on how

long the plume maintains its buoyancy, it will rise to a fairly high position in the atmosphere. However, strong turbulence

causes the plume to mix with the surrounding air, reducing plume temperature and buoyancy, eventually reaching a stable

80   layer at which the updraft stops (Damoah et al., 2006; Freitas et al., 2007). For these reasons, a significant amount of the

material emitted from biomass combustion is lofted above the surface, as compared with urban sources, the large majority of

which remain near the surface (Ichoku et al., 2008; Cohen and Prinn 2011). This point is important because if aerosol is

injected into the atmosphere above the planetary boundary layer (PBL) they can be carried by the faster free tropospheric

winds farther away, leading to a larger impact on the atmosphere (Vernon et al., 2018; Nelson et al., 2013).

85   The present generation of models has difficulty to reproduce the actual vertical distribution of atmospheric aerosols. One

reason stems from the fact that the in-situ production and removal mechanisms of aerosols as well as the distribution of rainfall

are not fully understood (Tao et al., 2012), all of which weaken the ability of simple models to reproduce the vertical

distribution of aerosols (Urbanski 2014; Cohen et al., 2017). In addition, heterogeneous aerosol processing associated with the

highly polluted conditions within the atmospheric plume may also change the hygroscopicity, which in turn impacts the

90   washout rate and vertical distribution of the aerosols (Kim et al., 2008; Cohen et al., 2011). On top of this, highly polluted

aerosol loadings, especially so for absorbing aerosols as found in fires, lead to changes in the radiative equations and the

vertical atmospheric stability (Guo et al., 2019; Cohen et al., 2018; Zhu et al., 2018). Furthermore, small scale convective

events and large-scale circulation patterns are generally not both well produced by the same scale models, leading to an

inherent bias against one or the other convection producing source (Winker et al., 2013; Jost et al., 2004). In summary these

95   factors can lead to actual changes in the vertical distribution of aerosols that simple models are not able to reproduce, in turn

affecting the distribution of aerosols hundreds to thousands of kilometers downwind.

This work describes a new approach to comprehensively understand global-scale, daily measurements of the vertical

distribution of aerosols, and introduces a simple modeling approach better capable of reproducing the vertical distribution of

smoke aerosols emitted by biomass burning. First, we analyze the plumes height from three and a half years of daily the

100   Multi-angle Imaging SpectroRadiometer (MISR) satellite measurements, separating the more than 67,000 measurements by

the magnitude of the measured variability. Next we build aerosol plume injection models depending on the region, terrain, land

type, and geospatial properties. We use this simple plume model to show that the aerosol injection heights are underestimated.

We then apply a linear statistical model and show that including measurements of column gas loadings from other satellites in

combination with the meteorological and FRP measurements produces a better match. We imply that ignoring the magnitude

105   of the source emissions is an important factor in the plume rise height, another factor which the current generation of models

does not take into consideration. We also demonstrate that improvements in the local convective transport process and direct

and semi-direct effects of aerosols are needed to further reduce the error between the models and measurements.

It is hoped that these results will provide insights to further improve our understanding of the vertical distribution of

aerosols, both from the modeling side, and from what sources of information are best required from the measurement

110   community to help the modelers improve their understanding. We also provide a unique perspective on the connections

between air quality and the vertical distribution of particulate matter, allowing the community make further advances in these

fields as well as associated issues of long-range transport of aerosols as well.

2 Methodology

2.1 MISR Aerosol Height Measurements

115   MISR, the Multi-angle Imaging SpectroRadiometer, is an instrument flying on the Terra satellite capable of recording

images at 9 different angles over 4 bands at 446nm, 558nm, 672nm, and 866 nm. The cameras point forward, downward, and

aftward, allowing images to be acquired with nominal view angles, relative to the surface of 0, ±26.1, ±45.6, ±60.0, and ±70.5

degrees. All cameras have a track width of 360 km and observations extending within ±81 degrees latitude (Khan et al., 2007).

In this paper, we use the MISR INteractive eXplorer (MINX) software, which captures the plume height from the MISR image

120   and combines it with the MODIS fire point measurements (also taken on the Terra satellite). The software then calculates the

wind speed and the elevation of contrast elements globally over a 1.1 km pixel area, providing a digitization of wildfire smoke

plume height (Val Martin et al., 2010; Kahn et al., 2007; Nelson et al., 2013).

2.2 Geography

Around the world, biomass burning and deforestation have undergone tremendous changes in the past few decades, with
125   current extremes making the news in many places throughout the world. To better interpret the land use conditions in the
biomass burning areas, we apply global land-cover type data of 18 different vegetation types, as measured in 2015 in Fig. 1.
We specifically focus on those areas where the land type has undergone known significant changes from forest to agriculture,
or from forest or agriculture to urban, as demonstrated in the black boxes in Fig. 1.

Considering MISR daily plume heights (where the 1.1km pixels are first averaged to 10km x 10km grids) throughout the
130   globe, we have determined that the respective average and standard deviation of the plume height over the three and a half
years of MISR daily measurements (from January 1 2008 through June 30 2011) are 1.37km and 0.72km. However, over our
regions of interest, we find that we are able to capture the large bulk of the standard deviation globally, as demonstrated in
Table S1.

The geographical data yields us a few conclusions about those regions which have the largest contribution to the biomass
135   burning height variation. First, they are distributed in the middle and low latitudes (between the Tropic of Cancer and the
Tropic of Capricorn) and/or high latitudes (near the Arctic Circle). Second, they tend to occur in regions of more rapid
economic growth, and/or in regions which are experiencing the most rapid change in land surface temperature.

2.3 MOPITT Carbon Monoxide (CO) Measurements

Carbon monoxide (CO) is a colorless and odorless gas that plays a major role in moderating the chemistry of the Earth's
140   atmosphere as well as having a deleterious effect on human health. One of the world's major sources of CO is emissions from
biomass burning. For these reasons, we obtain measurements of CO from the MOPITT satellite (an instrument mounted on
NASA's Terra satellite), which has collected data since March 2000. MOPITT's resolution is 22 km at nadir and observes the
Earth in swaths that are 640 km wide.

In specific we use all version 7, Level 2 daily data from January 1, 2008 through June 30, 2011, combining data from both
145   infrared channels (Deeter et al., 2013; Worden et al., 2010). This data has been demonstrated to provides an estimate of the
global distribution of CO in the troposphere (Worden et al., 2010). In reality, due to orbital conditions, aerosols, and clouds,
there is not entire coverage over all of our areas of interest each day. Therefore, we first average all MOPITT data to 1°x1°, and
secondly, we only use those values which subsequently have measurements from both MOPITT and MISR at the same time for
our inter-comparisons.

150   ### 2.4 OMI Nitrogen dioxide (NO₂) Measurements

Another chemical species co-emitted by biomass burning with aerosols and CO is NO_2 (Seinfeld and Pandis, 2006). For
this reason, we also use the daily average total column loading of NO_2 as measured by the Ozone Monitoring Instrument

(OMI). In specific we use version 3 Level 2 measurements taken from the Aura satellite (Boersma et al., 2007; Lamsal et al., 2011; Levelt et al., 2006), which detects the radiance spectra from 60 across-track pixels with ground pixel sizes ranging from
155   13kmx24km at nadir to about 13kmx150km at the outermost part of the swath.

One advantage of the OMI NO_2 column measurements is that they can often be observed under relatively cloudy or smoky conditions (Lin et al., 2014). Another advantage is that the atmospheric lifetime of NO_2 is only a few hours, and therefore the temporal-spatial distribution of the NO_2 column measurements is highly correlated with wildfire sources (Lin et al. 2019; Lan et al. 2019). NO_2 has another interesting property in that its production/emissions is a strong function of the
160   temperature at which the fires are burning, since NO_2 is formed based on the air temperature (Seinfeld and Pandis, 2006).

2.5 Plume Rise Model

Although emissions from biomass burning are similar to those from urban combustion sources, with the major difference being the much higher burning temperature. This ensures that a significant amount of the emissions from biomass burning will be transported upwards due to the positive buoyancy generated by the fire. Due to the confluence of both local and non-local
165   dynamical forcing in-situ, the ultimate height reached by these emissions is a complex function of the local fire energy and both the local and large-scale meteorology at the time of combustion. While the aerosol particles are immediately transported horizontally by the large-scale winds, their vertical rise will only stop once their local buoyancy has reached equilibrium, and any dynamical motion has degraded back to the background conditions (Freitas et al., 2007; Val Martin et al., 2018).

To approximate this rise, we use a simple plume rise model (Briggs, 1965) to generate the final injection height of the
170   biomass burning emissions based on the buoyancy and horizontal velocity of the plume and various atmospheric conditions. Although this model is based on an empirical formula mathematically, it is essentially a thermodynamic approximation (Cohen et al., 2018) which costs much less computationally as well as being quite efficient when the biomass burning source covers a large area.

In theory, if such an approach was successful, and it was given appropriate environmental data, it should be able to
175   reproduce the heights derived from the MISR multi-angle measurements. For this reason, we use a 1-D plume rise model to independently predict the position and height of each measured MISR plume at each 10km x10km grid which is found to have measurements. To initialize the model, we require meteorological data as well as MODIS hot-spot information.

2.6 NCEP Reanalysis Data

NCEP and NCAR produce an analysis/prediction system to produce a meteorological field analysis of the 6-hourly state
180   of the atmosphere from 1948 to the present. The measurements incorporated into this approach include ground based, in-situ, and remotely sensed sources, while the modeling aspect is based on state-of-the-art meteorological models. In specific, we obtain daily data for each day which we have MISR data, from reanalysis version 1 (Kalnay et al., 1996) .Specifically we use

the data required for us to run the plume rise model: the vertical temperature and pressure distributions, the surface air

temperature, and the initial vertical velocity of the smoke emissions (dP/dt). We then compute the vertical temperature gradient

185   (dT/dz) and the vertical velocity (dz/dt).

2.7 Regression Model

Linear regression is a simple method by which one can relate the impact that a set of orthogonal inputs have in terms or

reproducing measured environmental values. It does not imply causation, merely which the behavior acts in a similar manner.

However, when looking to describe whether or not a new variable has a significant amount of correlation with a given

190   phenomenon, it can be found to be very useful.

In this case, we are interested to see if the loadings of NO_2 and CO are related to the heights of the fires. There is a strong

physical case to be made here, since both are directly emitted by the fires themselves. Furthermore, the underlying causes of

these substances are different: NO_2 is a function of the fire temperature, while CO is a function of the Oxygen availability.

Furthermore, these are proxies for radiatively active substances such as soot and ozone.

195   For our work, we have decided to apply a simple linear regression model of the wind speed, FRP, CO, NO_2, and the ratio of

NO_2/CO. This is because the traditional plume rise models always include wind speed and FRP in their representations, so we

wanted to specifically include as many different representations of the co-emitted gasses as well, as given in Equations 1-7.

$$H_1 = \alpha * V_{wind} + \beta * W_{FRP} + \gamma * [CO] + \delta * [NO_2] + C \ , \tag{1}$$

$$H_2 = \alpha * V_{wind} + \beta * W_{FRP} + \gamma * [CO] + \varepsilon * ([CO]/[NO_2]) + C \ , \tag{2}$$

200    $$H_3 = \alpha * V_{wind} + \beta * W_{FRP} + + \delta * [NO_2] + \varepsilon * ([NO_2]/[CO]) + C \ , \tag{3}$$

$$H_4 = \alpha * V_{wind} + \beta * W_{FRP} + \gamma * [NO_2] + s \ , \tag{4}$$

$$H_5 = \alpha * V_{wind} + \beta * W_{FRP} + \gamma * [CO] + C \ , \tag{5}$$

$$H_6 = \alpha * V_{wind} + \beta * W_{FRP} + + \varepsilon * ([NO_2]/[CO]) + C \ , \tag{6}$$

$$H_7 = \alpha * V_{wind} + \beta * W_{FRP} + C \ , \tag{7}$$

205   We calculate all of the correlation coefficients ($R^2 > 0.2$) between the different models and the MISR measurements,

ensuring that ($P < 0.05$). Finally, we analyze both the magnitude of the regression coefficient as well as the magnitude of the

various best-fit terms. These models are then used to reproduce the aerosol heights and are ultimately compared with both the

plume model and the actual measurements.

3 Discussion and Results

210   We approach this problem with additional measurements compared to what are normally made so that we can have a deeper insight into how these somewhat related species have on height to which aerosols from biomass burning rise in the atmosphere. Due to the fact that there are additional processes in-situ which can lead to heating, cooling, and other changes to the dynamics, it is essential that we establish any first-effect relationships, and then work more deeply as a community to address them in turn.

215   First, we to enforce consistency, we impose a condition that for all days analyzed, we must have data present from all of the data sources: MISR, MODIS, MOPITT and OMI. On this basis, we explore the relationships between the two basic data sets (MISR and MODIS) and the source regions, as well as injecting additional information from MOPITT and OMI datasets without bias. Second, since these datasets make measurements with different assumptions, we also will reduce our bias in our inputs measurements as a function of clouds, different burning conditions, radiation feedbacks, and other actual atmospheric

220 effects. We hope that this will help us to more clearly clarify the actual atmospheric phenomena responsible for the vertical transport, which a more conventional plume rise model may not be able to account for.

3.1 Characteristics of MISR, OMI and MOPITT species

     We use a PDF analysis to look at the distribution of the daily fire-constrained aggregated Measurements from MISR from each region over the entire dataset from 2008 to 2011 in Fig. 2. The statistical mean and standard deviation over each region are

225 given in Table S1. We determine that the height of measurements ranges from 0 to 29 km, which is not only higher than previous studies (Cohen et al., 2018; Val Martin et al., 2018), but also includes some extreme events which have made their way into the stratosphere. Due to the fact that first, the majority of the plumes are injected into the boundary layer or the lower free troposphere, second that we are not looking into the underlying physics of stratospheric injection (Pengfei Yu et al., 2019), and third that plumes tend to accumulate within layers of relative atmospheric stability, we therefore want to set an upper

230 bound cutoff on the measured values that we will not consider after this point. Given the fact that the total percent of measurements over 5000m is less than 7.9%, we therefore only look at data with an upper limit of 5 km for the remainder of this work.

     We first observe that there are very different distributions of the measured heights over the different regions Fig. 2. The corresponding mean, standard deviation, and skewness of the heights over each respective region is given in Table S1. The

235 average percentage of the data which has a measured height above 2 km (selected because it is always in the free troposphere) is 15.0%, with the lowest in Central Canada of 41.7% and the highest in Midwest Africa of 0.8%. In terms of the amount of data measured with a height more than 4km, the average over the globe is 1.5%, while the range is as high as 6.6% in Central Canada and as low as 0.1% in Midwest Africa and Northern Australia. On the other end of the comparison, we also have some regions which are very polluted near the surface, while others show the vast majority of their heights are elevated off the

240   ground. Overall, we have a percentage of total plumes with a height below 200 m (the minimum rough level of the boundary

layer through the day) with a global mean of 2.3%, and a range from a minimum of 0.04% in Central Africa to 6.7% at Western

Siberia. Given these results, we need more deeply understand the driving factors across all of these different regions, as well as

the importance of biomass burning in terms of transporting aerosols through the boundary layer.

Second, we perform a comparison across the different daily time series of measured aerosol heights, CO column, and

245   NO_2 column as aggregated from January 1, 2008 to June 30, 2011 over all of the biomass burning regions Fig. S1. We consider

the burning season to be when we observe aerosol plumes and a peak in at least one of the CO and/or NO_2 column

measurements. This allows us to clearly demonstrate that the observed smoke peak is in fact due to burning of a significant

amount of material. In these cases, the peak occurs from November to March in Central Africa, Midwest Africa; June to

September in Central Canada, Eastern Europe, South America; April to July in Central Siberia; May to December in Southern

250   Africa, Northern Australia; January to April in Northern Southeast Asia; March to September in Siberia and North China;

April to September in West Siberia. In addition, the length of the peak burning time is also an important consideration which

varies greatly across the different regions. The length of the total number of burning days from the three and a half years of data

is an average is 108 days, with a minimum of 14 days in Eastern Siberia and a maximum of 388 days in Southern Africa.

Next, we look at the impact of FRP measurements and buoyancy in terms of the plume height distribution. In general, the

255   higher the FRP, the higher the plumes should rise. However, these measurements seem to include a larger number of total

measurements into the lower free troposphere than previous plume rise model studies have been able to account for. From our

measurements, we notice that the FRP (as computed on average over 1.1kmx1.1km grids where a fire exists) has a global mean

of 37.7W/m^2 and a reginal minimum and maximum of 31.1W/m^2 (Siberia and North China) and 82.6W/m^2 (Central Canada)

during the respective biomass burning seasons. Based on previous work, we would expect a general plume rise model to not be

260   able to match the observed heights well under these conditions, since the FRP is too low (Cohen et al., 2018; Gonzalez-Alonso

et al., 2019). One possible explanation for this phenomenon is that the biomass burning occurring during the times of year

where there is a negligible impact on the atmospheric loadings of NO_2 and/or CO is significantly more energetic and therefore

has a very different height profile, as compared to the times when the most emissions of NO_2 and/or CO are produced. Another

explanation is that there is additional forcing which are also playing a role in terms of the aerosol plume height rise that are

265   independent of the FRP. Yet another possibility (Mims et al., 2010; Val Martin et al., 2018) is related to there being some type

of problem with the presentation of the nature of the land-surface itself, since fires occurring in heavily forested and

agricultural areas are likely to have significantly different vertical distributions. Finally, it is possible that the intense aerosol

loadings themselves are leading to absorption of a significant amount of the IR radiation which is in turn biasing the FRP

measurements too low (Cohen et al., 2017; Cohen et al., 2018).

270   It is also possible that there are significant differences to be found in the non-linearity between FRP and the wind speed.

Interestingly, if the horizontal wind speed is quite high when the air passes over the fire source, it will cause turbulence and

vortices, resulting in a lifting force. On the other hand, if the wind speed is too high, it will bend the plume's momentum and reduce the upward transference based on any initial vertical injection velocity. Furthermore, the wind speed may have different relationships with convection, which itself plays a dominant role in the rise of the plume. Given these effects, we do not

275   directly consider wind-speed and the plume rise height independently, only within the confines of the plume rise model.

Since there are many underlying direct and indirect theoretical physical and chemical connections between the loadings of the CO and NO_2 and the overall plume heights from MISR, we want to investigate this possibility more deeply. To make this comparison, we first looked at the entire time series, not only those periods during which the measured aerosol heights obviously had an impact on the atmospheric loadings of the CO and NO_2. Next, we selected days which had data from all three

280   measurement sources: MISR, MOPITT, and OMI. Furthermore, since we could not find such a paper in the literature, we have decided to keep the relationship open and simple, without worry of over-constraining any relationship found. In theory, the injection height of the aerosol plume is related to the emission of smoke in the wildfires, since this is a function of the amount of heat released. Therefore, we would expect that higher emissions of CO and NO_2 should correspond to higher heights of aerosols. However, the formation mechanisms of these two trace gasses is different, with CO a function of oxygen availability

285   (and possibly surface wetness), while NO_2 is a function of the temperature of the burning. Furthermore, very high co-emitted levels of aerosols with the very high levels of trace gasses could also lead to a change in the vertical profile of the heating (Freitas et al., 2007).

To ensure that the variables are relatively independent, our analysis only considers only three mixtures of these species: the independent concentrations of CO, NO_2, and the multiple of the two with each other. We then investigate how changes in

290   the loadings of NO_2 and/or CO are associated with changes in the height of the plume. Furthermore, we need to consider the more extreme conditions in addition to the means, and are particularly interested in seeing how well loadings of the CO and NO_2 can be used to model those conditions where the plume heights are extreme.

In all of the regions of the world, with the exception of the case of NO_2 over Siberia and Northern China, we have a case where the mean value of the CO and NO_2 measurements is higher over the set of points where the actual FRP measurements

295   were made, than over the region as a whole Table 1. This is the point of this work, since we want to focus on the measured values from MOPITT and OMI which correspond to the same spatial locations as the measured FRP. This makes sense, since the magnitude of emissions from fires is very large compared with the non-burning season and/or surrounding areas. However, the differences in the CO are in generally smaller than for NO_2, which is further consistent with the fact that the lifetime of CO is much longer than that of NO_2. Thankfully the case is well understood over Siberia and North China is because there are some

300   known significant urban areas nearby to the burning regions. Furthermore, this exception occurs in winter, where we know there is a significant enhancement of NO_2 emissions due to the increase in urban biomass burning to offset the brutally cold winter conditions.

Over these fire-constrained points, we find that the variability of both CO and NO_2 remains very low when computed on a point-by-point basis. On the other hand, over the entire regions, the variability of the point-by-point measurements of both

305   NO_2 and CO are much higher. This is in large part due to the rapid changes in different land-use types in different parts of the regions of interest being studied (consistent with Cohen et al., 2018). These results are based on the statistics of more than 67000 daily MISR measurements. Therefore, for the remainder of the work, we only use the data for the NO_2 and CO which are obtained at points where FRP measurements exist.

Note that the measurements and the results here are looking at the aerosol heights measured over small spatial and

310   temporal domains. We are looking to analyze the impact of the initial plume rise, and any very rapid adjustments in the atmosphere. The plume heights, both measured and modeled are not consistent with large-scale transport due to meteorology, factors enhancing the stability of a layer or changing the chemistry within a plume. They certainly are not receptive to a Lagrangian type of modeling effort, which is supposed to be focused on the air itself and in particular air at the large scale. Therefore, the results given here show here are the best methods currently used to reproduce the spatial distribution of aerosol

315   plumes produced by wildfires.

3.2 Plume Rise Model Applied to MISR and Meteorological Measurements

The annual average global total cumulative FRP from 2008 to 2011 is 209MW, based on more than 16000 measured MODIS fire hotspots. Overall, the measured FRP has been shown to be on the rise in recent years (Cohen 2018; Freeborn et al., 2014), although there is still a fundamental and significant amount of underestimation based on the current measurement

320   techniques (Giglio et al., 2006). The plume rise model in theory should take these FRP values, and combine them with knowledge of the vertical thermal stability and the wind speed, to approximate the height to which the plume ultimately rises at equilibrium with its environment.

However, in reality, direct and semi-direct effects are not considered when using the simple plume rise model, although they are known to be important (Tao et al., 2012). Therefore, a different approach which attempts to take these forcings and/or

325   the underlying aerosol loadings into account may lead to a better representation of the plume height rise, if such a model can be parameterized. Furthermore, the plume rise model relies on the atmospheric stability, and therefore does not take into account rainfall, changes in fire burning, in-situ chemical and physical production and removal, as well as the afore mentioned interactions radiatively between the aerosol and the atmospheric environment.

All of these shortcomings aside, the use of simple plume models is the current scientific standard approach, and therefore

330   we will apply it here as well. This is done by first aggregating the daily statistics of the vertical aerosol height over all parts of each region of interest Table 2. Direct comparisons are made between the modelled heights and the measured heights, and we discard all model results which are more than 0.25km different from each other. Overall 5 of the 14 regions studies in this work were shown to have a good match: West Siberia; Alaska; Central Canada; Argentina; Eastern Europe, where the modelled (and

measured average heights) respective are 0.79 km (0.95 km) 1.39 km (3.03 km), 1.73 km (2.19 km), 0.65 km (0.25 km), 1.27

335 km (2.67 km).

Next, we look at the difference from day-to-day at each of the sites which has satisfied the overall requirement. The mean daily difference between the plume rise model and the MISR measurements as a whole show a large amount of variation, with a global average of 0.44, a maximum of 1.13 km (in West Siberia), and a minimum of 0.04 km (in Argentina). Across all of the different regions we find that the plume rise model underestimates the plume height. Hence, these differences are not normally

340 distributed, and are strongly indicative of a bias. In addition to this, we compute the RMS error Table 3 as a way of quantifying overall how well the data. The RMS is found to be considerably larger than the difference of the means, indicating that a small number of extreme values are dominating the overall results, which were found to be 0.67 km, 0.88 km, 1.36 km, 0.40 km, and 0.85 km in the respective five areas.

To more carefully determine the extent of any bias, we analyze the PDF of the model and measurement results Fig. S2.

345 This approach yields a clear determination that the plume rise model consistently underestimates the measured injection height, with the underestimate ranging from 6% (in Argentina) to 66% (in Southern Africa), and a global average of 33%. However, if we constrain ourselves to those fires occurring only in heavily forested regions, the average underestimate is reduced considerably to 11%. On the other hand, if we look across Africa as a whole, we find that the underestimate is on average 52%, a finding which deviates more from the measured aerosol vertical distribution than previous global studies (Val

350 Martin et al., 2018) as well as those over Southeast Asia (which previously has been considered one of the world's worst performing regions for such plume rise models, such as Reid et al., 2013; Cohen, 2018).

Furthermore, even though the plume rise model leads to a low bias compared with the measured height, it is still not ideal for very low plumes which are found near the surface. The plume rise model tends to instead uniformly overestimate the amount of aerosol found in the upper parts of the boundary layer from 0.5km to 1.5km, while at the same time not providing

355 any reliable amount of prediction for the cases where there is a considerable amount of aerosol under 0.5km. For example, the plume rise model is sometimes a good fit for aerosol heights under 0.5 km such as in West Siberia and Eastern Europe (where 23.5% and 12.3% of the measurements are under 0.5km and 27% and 13.6% of the plume rise model heights are under 0.5km, respectively). However, in other locations, the plume rise model grossly overestimates the amount under 0.5km such as in Central Africa and East Siberia (where 3.6% and 17.9% of the measurements are under 0.5km and 20.5% and 51.0% of the

360 plume rise model heights are under 0.5km, respectively). In the case of Argentina there is a slight underestimate of the 0.5km heights by the plume rise model (49.4% of measurements and 30.1% of the plume rise model heights). One of the reasons for this is that in general the plume rise model tends to underestimate the results from 1.5km to 2.5km, and cannot reproduce results reliably at all above 2.5km. This is partly due to the effect that the FRP values are too low, and possibly due to other processes occurring in-situ which further lead to buoyancy and/or convection.

365   A few special regions of interest have been observed when comparing the plume rise results with the measurements. In Southern Africa plumes cover 9763-pixels or 19% of the total research area, and therefore are extremely representative of the overall atmospheric conditions. What is observed is that there is almost no aerosol (only 5.9%) present close to the ground (from 0km to 1km). The vast majority of the aerosols, 92.6%, are concentrated from 1km to 3km. Furthermore, we observe that the time series of both CO and NO_2 loading is significantly higher than other regions Fig. S1. This finding is completely the

370 opposite form the plume rise model result, which shows that most of the pollutants (97%) are concentrated in the range of 0-1km, while almost none (3%) is found from 1km to 3km. There are a few reasons for this finding. First of all, when both CO and NO_2 loadings are high, the aerosol concentration and AOD will also be high, since they are co-emitted at roughly similar ratios from the fires. This in turn will both lead to a further underestimation of the FRP due to the outwelling infrared which is partially absorbed by the aerosols, as well as provide a further uplifting energy source due to the semi-direct effect (Tao et al.,

375 2012; Guo et al., 2019). In other words, the assumptions underlying the plume rise model may not be completely relevant or dominant over this region under these conditions.

     A second special region, which completely contrasts with Southern Africa is found in Argentina. In this region, a much smaller amount of the total research area is covered in plumes of 1063-pixels or 2.1%. A large amount of the total aerosol (83.8%) exists below 1km, while only a small amount (5.1%) is found above 2km. In this case, the plume rise model achieved

380 its best match globally, with a large amount (92.2%) found below 1km and a small amount (0.35%) found above 2km. Furthermore, the loadings of CO and NO2 are both considerably low as compared to other regions studied in this work. It is under these relatively lesser polluted, fewer and less intense fires, and lower density of total surface area burning, that the plume rise model can achieve its best results, implying that small-scale fires truly are dominant over this region, and that the model is reasonable to use in such a region. Although it is still obvious that even in this best result case, that the plume rise

385 model is fundamentally biased towards the aerosol vertical distribution being too low, especially the amount into the free troposphere.

     As we have observed, the simple plume rise models based on Briggs, 1965, are useful under specific circumstances. This is especially the case when the atmosphere is relatively stable, the total loading of pollutants is not too large (i.e. there is fewer fire masking and less of the semi-direct effect to contend with), and where the density of fires is lower (and hence there is less

390 overall buoyancy changing the atmosphere's dynamics). On top of this, more flat and uniform areas are less likely to have local convection, further leading to an improvement of the effectiveness of the simple plume rise model. It is for these many reasons why we find that the simple plume rise model does not provide an ideal fit over many regions, and for this reason, we propose a simple statistical model as an alternative.

3.3 Regression Model Applied to MISR, OMI, MOPITT and Meteorological Measurements

395   Since plume rise models rely solely on information related to fire intensity and meteorological conditions in order to compute an aerosol injection height, we want to build a relationship that also includes the net effects of pollutants as well. Therefore, we introduce and globally apply seven different combinations of relationships between FRP, Wind, CO, NO_2 and injection height Eq.1-7. Different combinations of CO and NO_2 are applied to the linear regression model. CO and NO_2 are independently mixed with the meteorological terms in Eq.4 and Eq.5, while they are jointly mixed together with the

400   meteorological terms in Eq.1. A non-linear weighted variable of NO_2/CO is mixed on its own with the meteorological variables in Eq.6, while it is mixed with either one of CO and NO_2 in Eq.2 and Eq.3. The reason for this is that there is a significant physical relevance for determining how much NO_2 is emitted per unit of CO, which is a strong function of the fire temperature as well as Oxygen availability. This set of models is capable of providing a clear relationship between the response of either or both of CO and NO_2. Such an approach allows for us to examine the strengths and weaknesses of each combination

405   in terms of the spatial-temporal distribution of the measured heights, as well as the contribution to the absolute magnitude.

The average statistical error and average statistical correlation (coefficient of determination, R^2) between the datasets used to determine the best-fit coefficients for α, β, γ, δ and ε, with the resulting statistics displayed in Table 2. While a comparison of the time series of the region-averaged injection height was made over all 14 regions. When different linear combinations are evaluated for their correlation against the MISR measurements, an optimal combination is selected and

410   considered to be a success only if $R^2>0.2$ and the $P<0.05$. Furthermore, we compare the modeled average injection height in an absolute sense to the measured values, and retain the data if the difference is smaller than 0.25km. Based on these results, the best-fit model-predicted injection height and the measured averaged injection height were found to be reasonable only at 8 different sites.

In general, when CO or NO_2 or both are included in these different combinations for these regions, the normalized

415   coefficients of CO and NO_2 have a larger value than the respective normalized coefficients of FRP or wind speed. This means that when these variables occur simultaneously, the contaminants have a stronger influence on the final injection height of the plume. This is found to especially be the case in regions which have higher loadings of pollution.

This comparison also is found to be valid in regions which in general are less polluted. For example, even in relatively clean Central Canada, the linear combination of NO_2 and the ratio of NO_2 and CO produces the best fit, with the coefficient of NO_2

420   being roughly an order of magnitude larger (at 3.2×10^3) as compared to the coefficients of FRP and Wind (which are respectively a magnitude of order smaller, at 3.3×10^2 and -2.3×10^2).

3.4 Comparison between the Plume Rise Model and the Regression Model

The results in Table 3 indicate that inclusion of either one of CO and NO_2 or in some cases both, always provides a better fit to the measured vertical heights when using the regression aerosol height rise model, as compared with those model cases

425   where the loadings of the gasses are excluded. In addition, the fit is better over a larger number of regions (8 regions versus 5 regions), details are shown in Fig. S3. What we observe is that the regression model does relatively better in regions which are more polluted, while the plume rise model does relatively better only in regions which have very low amounts of burning in terms of FRP. A detailed look at the day by day values from the MISR measurements of aerosol height, the regression model of aerosol height, and the plume rise model are given in Fig. 3.

430   As shown in Fig. 3 there are three regions where both modeling approaches work well. In West Siberia, the regression model shows more stability than plume rise model, with the results more narrowly concentrated around 1000m. Furthermore, the results are mostly found within the range of the measured variation. The plume rise models results are also relatively stable, although more dispersed in general than the regression model. Overall the RMS is 0.47 between the measured values and the regression model, while it is 0.67km between the measured values and the plume rise model. A similar set of results is found in

435   Alaska, with the RMS for the regression modeling being 0.88km and that of the plume rise model being 0.77km. The major difference here is that the plume rise model results have a variance higher than that of the measurements (SD of 0.91km for the regression model and 3.03km for the plume rise model). In the case of Central Canada, although both modeling approaches have a decent fit, there is a clear difference between their overall performance. In general, the results of the plume rise model (1.73km) are biased significantly lower than both the measurements (1.97km) and the regression model (2.13km), while there

440   is little bias between the measurements and the regression model. To make this point clear, only roughly 7.9% of the measured results are outside of 1 standard deviation from the measured mean, while 50% of the plume rise model results and 43% of the regression model results are found to be outside of the 1 standard deviation from the measured mean. Note that this is the sight which has the highest RMS error and still yields a successful fit for both modeling approaches. Details are given in Fig. S4.

        In some of the more highly polluted regions, the regression model showed a decent performance, while the plume rise

445   model did not. The overall goodness of the fit of the regression model is reasonable in the cases of South America, Siberia and North China, Northern Southeast Asia, and Northern Australia. This is because these areas emit large amounts of CO and NO_2, in some cases solely during the biomass burning season, and in other cases due to a combination of biomass burning and urban sources. Overall in these more polluted regions, the regression model is found to have little bias (respectively -0.02km, -0.20km, -0.22km, and 0.15km), which helps to establish the predictive ability of using the gas loadings in terms of predicting

450   the vertical distribution of the aerosol heights.

        Although the vertical distribution of aerosol cannot be successfully simulated at all sites by using the regression model approach, at the sites where it provides a reasonable fit, it seems to do better than the plume rise model approach. This improvement is found in terms of both the bias and the RMS. Under true world conditions, there is a significant impact of co-emitted aerosols and/or heat. These changes either directly alter the heating throughout the profile as well as indirectly

455   introduce a negative bias on measurements of the FRP below. No matter the underlying specific reasons, overall, we find that the regression model approach yields at least as good if not a more precise representation of the plume rise height as compared

with the simple plume rise model. However, combining the two approaches yields the best overall result, since there are some locations in which each approach is better than the other approach.

What is most important to note is that in some of the regions, none of these simple approaches work. This is particularly

460   so for when the measured distribution of the aerosol heights is when there is a diverse set of sources. For example, in Africa there are significant sources from biomass burning, as well as from rapid urbanization and burning over many different land use types and under many different types of conditions. Another potential problem occurs when there may be a significant amount of smoke which has been transported from another region, such as the exchange of smoke between the Maritime Continent and Northern Australia. Furthermore, both approaches will not tend to work well under conditions in which the

465   atmosphere is not highly stable, or has a high variation in weather conditions. Under these conditions, a more complex modeling approach and the improvement of measured fire data.

4 Conclusions

This work quantifies the measured values of the aerosol vertical distribution over biomass burning areas of the Earth on a daily basis from January 2008 through June 2011. We find that there is a significant amount of total aerosol which reaches the

470   free troposphere, as well as large amounts which are not uniformly distributed throughout the boundary layer, both of which are not readily explained by first order theoretical approximations and present-day community-standard models.

To address these issues, we introduce a new approach, based on remotely sensed measurements of fire properties, wind, and column loadings of NO_2 from OMI and CO from MOPITT to constraining the aerosol heights over different geographic regions. This approach is based on the physical concept that the emissions of aerosols and the height to which they rise should

475   be related to other co-emitted species like NO_2 and CO and the co-emitted heat, which is also a function of the ratios of NO_2 and CO produced by the burning. Our results are compared against both the measured MISR height values as well as basic plume rise model computations using the same fire radiative power and meteorological datasets.

Our results indicate that our new method reproduced the measured values significantly better over much of the world in terms of reproducing the measured vertical distribution as compared with the simpler plume rise approach. In specific, we find

480   that applying the plume rise model leads to a model underestimation of the measured MISR heights overall, whereas our approach, where it works, does not exhibit such a bias. This finding is consistent with the fact that FRP is underestimated globally, in part due to clouds and aerosols, and in part due to sampling and other issues. We also find that the plume rise model tends to be too narrowly confined compared with the regression model and the modeled results. However, the plume rise model does better in terms of reproducing the aerosol injection height when it is solely contained and well mixed within the

485   atmospheric boundary layer, but for higher altitudes, the model capability is poor. The average underestimation of the plume rise model injection height is 33%. On the other hand, the regression model has an overall improved the accuracy of the

measured results, in particularly doing a better job reproducing results in the free troposphere. The regression model is also more widely applicable around the globe, with the number or regions successfully simulated increasing from five to eight.

490 In specific, we find that the plume rise model works well in regions which are not frequently cloud covered during the local biomass burning seasons, in particularly so over non-tropical forested regions. In specific, the plume rise model has its greatest successes in Alaska (RMS error of 0.77km for the regression approach versus 0.88km for the plume rise model approach), Argentina (the regression model approach does not succeed versus and RMS error of 0.40km for the plume rise model approach), and Western Siberia (RMS error of 0.47km for the regression approach versus 0.67km for the plume rise model approach). In most of the other parts of the world, the regression model approach is much better at reproducing the 495 vertical distribution than the plume rise model, even including some major extreme events including the release of aerosols into the stratosphere, and tends to do so with a reasonably lower RMS error and low standard deviation.

One of the major advantages of the regression model approach is that it is more capable of picking up those cases where aerosols are lofted into the lower free troposphere, and another advantage stems from its ability to reproduce better those cases where the near surface is clean, but the upper part of the boundary layer is polluted. In the cases of Eastern Siberia and Amazon 500 South America, we find that the regression model performs reasonably well, while the plume rise model does not succeed. In the case of Northern Australia, the regression model is capable of reproducing the aerosol height with a relatively reasonable set of statistics, although the measurements in this region are found to be very unique; sometimes the plume is mainly concentrated in the lower free troposphere and is local in nature, while other times it is found in the upper troposphere and lower stratosphere, in which case it is thought to be transported from the Maritime Continent. We also find that the regression 505 model works well in two other special cases. The first is the case of Siberia and Northern China, where there is a considerably large amount of local urban pollution which is mixed into the biomass burning plumes. The second is the case of Northern Southeast Asia, where there are both large amounts of local pollution as well as considerable issues with extensive cloud cover.

Based on these results and in specific where both modeling approaches fail, we have come up with a list of recommendations for how to improve the reproduction of the vertical aerosol distribution in the future. First, improving the 510 accuracy of FRP measurements, especially so under cloud and heavily polluted conditions. Secondly, improving the ability of simple models to compensate for the impact of local-scale radiative forcings, deep convection, aerosol-radiation interactions and aerosol-cloud interactions. Based on our overall results, we believe that an improvement can be made to the current generation of GCMs, atmospheric chemical transport models, and remote sensing inversions, all of which depend on a more precise knowledge of the aerosol vertical distribution.

515 **Author Contributions**

Shuo Wang: data curation, formal analysis, investigation, software, visualization, writing – original draft.

Jason Blake Cohen: conceptualization, funding acquisition, investigation, methodology, project administration, resources,

supervision, validation, writing – original draft, review & editing.

Chuyong Lin: data curation, investigation, software.

520 Weizhi Deng: software, visualization.

Code/Data availability: All processed data, results, and codes are freely available for download at
https://doi.org/10.6084/m9.figshare.10252526.v1

Conflict of Interest: The authors declare that they have no conflict of interest.

Acknowledgements

525 We would like to acknowledge the PIs of the MISR, MOPITT, and OMI instruments for providing the remote sensing
measurements, and NCEP reanalysis project for providing the meteorology measurements. MISR data was obtained from
https://misr.jpl.nasa.gov/getData/accessData/, MOPITT data was obtained from https://eosweb.larc.nasa.gov/datapool. OMI
data was obtained from https://disc.gsfc.nasa.gov/mirador-guide?tree=project&project=OMI, and NCEP data was obtained
from https://www.esrl.noaa.gov/psd/data/gridded/data.ncep.reanalysis.html. The work was supported by the Chinese National

530 Young Thousand Talents Program (Project 41180002), the Chinese National Natural Science Foundation (Project 41030028),
and the Guangdong Provincial Young Talent Support Fund (Project 42150003).

References

Achtemeier, G. L., Goodrick, S. A., Liu, Y., Garcia-Menendez, F., Hu. Y., and Odman, M. T.: Modeling Smoke Plume-Rise
and Dispersion from Southern United States Prescribed Burns with Daysmoke, Atmosphere, 2, 358-388,
535 doi:10.3390/atmos2030358, 2011.
Briggs, G. A.: A plume rise model compared with observations. J. Air Pollut. Con. Assoc., 15, 433–438,
doi:10.1080/00022470.1965.10468404, 1965.
Boersma, K.F., Eskes, H.J., Veefkind, J.P., Brinksma, E.J., Van Der A, R.J., Sneep, M., Van Den Oord, G.H.J., Levelt, P.F.,
Stammes, P., Gleason, J.F., and Bucsela, E.J.: Near- real time retrieval of tropospheric NO2 from OMI, Atmos. Chem. Phys.,
540 7, 2103–2118, doi:10.5194/acp-7-2103-2007, 2007
Chew, B. N., Campbell, J. R., Salinas, S. V., Chang, C., W., Reid, J. S., Welton, E. J., and Liew, S. C.: Aerosol particle
vertical distributions and optical properties over Singapore, Atmos. Environ., 79, 599–613,
doi:10.1016/j.atmosenv.2013.06.026, 2013.
Cohen, J. B. and Prinn, R. G.: Development of a fast, urban chemistry metamodel for inclusion in global models, Atmos.
545 Chem. Phys., 11, 7629–7656, doi:10.5194/acp-11- 7629-2011, 2011.
Cohen, J. B.: Quantifying the occurrence and magnitude of the Southeast Asian fire climatology, Environ. Res. Lett., 9,
114018, doi:10.1088/1748-9326/9/11/114018, 2014.
Cohen, J. B. and Wang, C.: Estimating global black carbon emissions using a top-down Kalman Filter approach, J. Geophys.
Res.-Atmos., 119, 307–323, doi:10.1002/2013JD019912, 2014.
550 Cohen, J. B., Lecoeur, E., and Hui Loong Ng, D.: Decadal-scale relationship between measurements of aerosols, land-use
change, and fire over Southeast Asia, Atmos. Chem. Phys., 17, 721-743, doi:10.5194/acp-17-721-2017, 2017.
Cohen, J. B., Hui Loong Ng, D., Lim, A. W. L., and Xin R. C. J.: Vertical distribution of aerosols over the Maritime
Continent during El Niño, Atmos. Chem. Phys., 18, 7095-7108, doi: 10.5194/acp-18-7095-2018, 2018.
Damoah, R., Spichtinger, N., Servranckx, R., Fromm, M., Eloranta, E. W., Razenkov, I. A., James, P., Shulski, M., Forster,

555   C., and Stohl, A.: A case study of pyro-convection using transport model and remote sensing data, Atmos. Chem. Phys., 6,
        173– 185, doi:10.5194/acp-6-173-2006, 2006.

        Deeter, M. N., Martínez-Alonso, S., Edwards, D. P., Emmons, L. K., Gille, J. C., Worden, H. M., Pittman, J. V., Daube, B. C.,
        and Wofsy, S. C.: Validation of MOPITT Version 5 thermal- infrared, near-infrared, and multispectral carbon monoxide pro-
        file retrievals for 2000–2011, J. Geophys. Res., 118, 6710–6725, doi:10.1002/jgrd.50272, 2013.

560   Dewitt, H. and Gasore, J.: Seasonal and diurnal variability in O3, black carbon, and CO measured at the Rwanda Climate
        Observatory, Atmos. Chem. Phys., 19, 2063-2078, doi:10.5194/acp-19-2063-2019, 2019.

        Freitas, S. R., Longo, K. M., Chatfield, R., Latham, D., Silva Dias, M. A. F., Andreae, M. O., Prins, E., Santos, J. C., Gielow,
        R., and Carvalho Jr., J. A.: Including the sub-grid scale plume rise of vegetation fires in low resolution atmospheric transport
        models, Atmos. Chem. Phys., 7, 3385–3398, doi:10.5194/acp- 7-3385-2007, 2007.

565   Field, R. D., van der Werf, G. R., and Shen S. P. P.: Human amplification of drought-induced biomass burning in Indonesia
        since 1960, Nat. Geosci., doi:10.1038/ngeo443, 2009.

        Freeborn, P. H., Wooster, M. J., Roy, D. P., and Cochrane, M. A.: Quantification of MODIS fire radiative power (FRP)
        measurement uncertainty for use in satellite-based active fire characterization and biomass burning estimation, Geophys. Res.
        Lett., 41, 1988–1994, doi:10.1002/2013GL59086, 2014.

570   Giglio, L., Csiszar, I., and Justice, C. O.: Global distribution and seasonality of active fires as observed with the Terra and
        Aqua Moderate Resolution Imaging Spectroradiometer (MODIS) sensors, J. Geophys. Res.-Biogeo., 111, G02016,
        doi:10.1029/2005JG000142, 2006.

        Gonzalez, L., Val Martin, M., and Kahn, R. A.: Biomass-burning smoke heights over the Amazon observed from space,
        Atmos. Chem. Phys., 19. 1685-1702. 10.5194/acp-19-1685-2019, 2019.

575   Guo, J., Deng, M., Lee, S. S., Wang, F., Li, Z., Zhai, P., Liu, H., Lv, W., Yao W., and Li X.: Delaying precipitation and
        lightning by air pollution over the Pearl River Delta. Part I: Observational analyses, J. Geophys. Res., 121, 6472-6488, doi:
        10.1002/2015JD023257, 2016

        Guo, J., Li, Y., Cohen, J. B., Li, J., Chen, D., Xu, H., Liu, L., Yin, J., Hu, K., and Zhai, P.: Shift in the temporal trend of
        boundary layer height trend in China using long-term (1979–2016) radiosonde data. Geophysical Research Letters, 46,
580   6080-6089, doi:10.1029/2019GL082666, 2019.

        Husar, R. B., Prospero, J. M., and Stowe, L. L.: Characterization of tropospheric aerosols over the oceans with the NOAA
        advanced very high resolution radiometer optical thickness operational product, J. Geophys. Res., 102, 16889–16909, doi:
        10.1029/96jd04009, 1997.

        Ichoku, C., and Ellison, L.: Global top-down smoke-aerosol emissions estimation using satellite fire radiative power
585   measurements, Atmos. Chem. Phys., 14, 6643–6667, doi: 10.5194/acp-14-6643-2014, 2014

        Ichoku, C., Giglio, L., Wooster, M., and Remer, L.: Global characterization of biomass-burning patterns using satellite
        measurements of fire radiative energy, Remote Sens. Environ., 112, 2950–2962, doi: 10.1016/j.rse.2008.02.009, 2008.

        Jost, H., Drdla, K., Stohl, A., Pfister, L., Loewenstein, M., Lopez, J. P., Hudson, P. K., Murphy, D. M., Cziczo, D. J., Fromm,
        M., Bui, T. P., Dean-Day, J., Gerbig, C., Mahoney, M. J., Richard, E. C., Spichtinger, N., Pittman, V. J., Weinstock, E. M.,
590   Wilson, J. C., and Xueref, I.: In-situ observations of mid-latitude forest fire plumes deep in the stratosphere, Geophys. Res.
        Lett., 31, L11101, doi:10.1029/2003GL019253, 2004.

        Kahn, R. A., Li, W. H., Moroney, C., Diner, D. J., Martonchik, J. V., and Fishbein, E.: Aerosol source plume physical
        characteristics from space-based multiangle imaging, J. Geophys. Res., 112, D11205, doi:10.1029/2006JD007647, 2007.

        Kalnay, E., Kanamitsu, M., Kistler, R., Collins, W., Deaven, D., Gandin, L., Iredell, M., Saha, S., White, G., Woollen, J., Zhu,
595   Y., Chelliah, M., Ebisuzaki, W., Higgins, W., Janowiak, J., Mo, K. C., Ropelewski, C., Wang, J., Leetmaa, A., Reynolds, R.,
        Jenne, R., and Joseph, D.: NCEP/NCAR 40-year reanalysis project, Bull. Amer. Meteor Soc., 1996, 77,437-472, doi:
        10.1175/1520-0477(1996)077<0437:TNYRP>2.0.CO;2, 1996.

        Kauffman, J. B., Steele, M. D., Cummings D. L., and Jaramillo V. J.: Biomass dynamics associated with deforestation, fire,
        and, conversion to cattle pasture in a Mexican tropical dry forest, For. Ecol. Manage., 176, 1-12, doi:
600   10.1016/s0378-1127(02)00227-x, 2003.

        Kim, D., Wang, C., Ekman, A. M. L., Barth, M. C., and Rasch, P.: Distribution and direct radiative forcing of carbonaceous
        and sulfate aerosols in an interactive size-resolving aerosol-climate model, J. Geophys. Res., 113, D16309,

doi:10.1029/2007JD009756, doi:10.3390/rs5094593, 2008.

Labonne, M., Bréon, F.-M., and Chevallier, F.: Injection height of biomass burning aerosols as seen from a spaceborne lidar,
605   Geophys. Res. Lett., 34, doi:10.1029/2007GL029311, 2007.

Lamsal, L. N., Martin, R. V., Padmanabhan, A., van Donkelaar, A., Zhang, Q., Sioris, C. E., Chance, K., Kurosu, T. P., and
    Newchurch, M. J.: Application of satellite observations for timely updates to global anthropogenic NOx emission inventories,
    Geophys. Res. Lett., 38, doi:10.1029/2010GL046476, 2011.

Lan, R. Y., Cohen, J. B., Lin, C. Y., and Loong, D. H.: Integrating Multiple Satellites with Models Reveals Southeast Asian
610   Biomass Burning Emissions in 2016 is More Than Double Present Inventories, submitted and under review, see attachment.

Leung, F. Y. T., Logan, J. A., Park, R., Hyer, E., Kasischke, E., Streets, D., and Yurganov, L.: Impacts of enhanced biomass
    burning in the boreal forests in 1998 on tropospheric chemistry and the sensitivity of model results to the injection height to
    emissions, J. Geophys. Res., 112, D10313, doi:10.1029/2006JD008132, 2007.

Levelt, P. F., van den Oord, G. H. J., Dobber, M. R., Malkki, A., Visser, H., de Vries, J., Stammes, P., Lundell, J. O. V., and
615   Saari, H.: The ozone monitoring instrument, Ieee Trans. Geosci. Remote Sens., 44, 1093–1101, doi:Urn:nbn:nl:ui:25-648485,
    2006.

Lin, C. Y., Wang, S., Lan, R. Y., and Cohen, J. B.: Application of a Simple Variance Maximization Technique to MOPITT
    CO Column Data, and Resulting Improved Representation of Biomass Burning and Urban Air Pollution Sources, submitted
    and under review, see attachment.

620 Lin, N. H., Sayer, A. M., Wang, S. H., Loftus, A. M., Hsiao, T. C., Sheu, G. R., and Chantara, S.: Interactions between
    biomass- burning aerosols and clouds over Southeast Asia: Current status, challenges, and perspectives, Environ. Pollut., 195,
    292–307, doi: 10.1016/j.envpol.2014.06.036, 2014.

Mims, S. R., Kahn, R. A., Moroney, C. M., Gaitley, B. J., Nelson, D. L., and Garay, M. J.: MISR stereo-heights of grassland
    fire smoke plumes in Australia, IEEE Trans. Geosci. Remote Sens., 48, 25–35, doi:10.1109/TGRS.2009.2027114, 2010.

625 Nelson, D. L., Garay M. J., Kahn R. A., and Dunst B. A.: Stereoscopic Height and Wind Retrievals for Aerosol Plumes with
    the MISR INteractive eXplorer (MINX), Remote Sens., 5, 4593– 4628, doi:10.3390/rs5094593, 2013.

Paugam, R., Wooster, M., Freitas, S., and Val Martin, M.: A review of approaches to estimate wildfire plume injection height
    within large-scale atmospheric chemical transport models. Atmos. Chem. Phys., 16, 907–925, doi:10.5194/acp-16-907-2016,
    2016.

630 Petersen, W. and Rutledge, S.: Regional variability in tropical convection: observations from TRMM, J. Climate, 14, 3566–
    3586, doi:10.1175/1520-0469(1989)046<0037:OOLFOI>2.0.CO;2, 2001.

Petrenko, M., Kahn, R. A., Chin, M., Soja, A. J., Kucsera, T., and Harshvardhan: The use of satellite-measured aerosol
    optical depth to constrain biomass burning emissions source strength in the global model GOCART, J. Geophys. Res.,
    doi:10.1029/2012JD017870, 2012.

635 Pfister, G. G., Wiedinmyer, C., and Emmons, L. K.: Impacts of the fall 2007 California wildfires on surface ozone:
    Integrating local observations with global model simulations, Geophys. Res. Lett., 35, L19814, doi: 10.1029/2008GL034747,
    2008.

Reid, J. S., Hyer, E. J., Johnson, R. S., Holben, B. N., Yokelson, R. J., Zhang, J. L., Campbell, J. R., Christopher, S. A., Di
    Girolamo, L., Giglio, L., Holz, R. E., Kearney, C., Miettinen, J., Reid, E. A., Turk, F. J., Wang, J., Xian, P., Zhao, G.,
640   Balasubramanian, R., Chew, B. N., Janjai, S., Lagrosas, N., Lestari, P., Lin, N. H., Mahmud, M., Nguyen, A. X., Norris, B.,
    Oanh, N. T. K., Oo, M., Salinas, S. V., Welton, E. J., and Liew, S. C.: Observing and understanding the Southeast Asian
    aerosol system by remote sensing: An initial review and analysis for the Seven Southeast Asian Studies (7SEAS) program,
    Atmos. Res., 122, 403–468, 2013.

Rogers, R. R., Hostetler, C. A., Hair, J. W., Ferrare, R. A., Liu, Z., Obland, M. D., Harper, D. B., Cook, A. L., Powell, K. A.,
645   Vaughan, M. A., and Winker, D. M.: Assessment of the CALIPSO Lidar 532 nm attenuated backscatter calibration using the
    NASA LaRC airborne High Spectral Resolution Lidar, Atmos. Chem. Phys., 11, 1295–1311, doi:10.5194/acp-11-1295-2011,
    2011.

Steinfeld, J. H. and Pandis, S. N.: Atmospheric chemistry and physics: from air pollution to climate change, Environment,
    Phys. Today, 40, 26-26, doi:10.1063/1.882420, 2006.

650 Singh, N., Banerjee, T., Raju, M. P., Deboudt, K., Sorek-Hamer, M., Singh, R. S., and Mall R. K.: Aerosol chemistry,

transport, and climatic implications during extreme biomass burning emissions over the Indo-Gangetic Plain, Atmos. Chem. Phys., 18, 14197-14215, doi:10.5194/acp-18-14197-2018, 2018

Spracklen, D. V., Mickley, L. J., Logan, J. A., Hudman, R. C., Yevich, R., Flannigan, M. D., and Westerling A. L.: Impacts of climate change from 2000 to 2050 on wildfire activity and carbonaceous aerosol concentrations in the western United States,
655   J. Geophys. Res.,114, D20301, doi:10.1029/2008JD010966, 2009.

Tao, W.-K., Chen, J.-P., Li, Z., Wang, C., and Zhang, C.: Impact of aerosols on convective clouds and precipitation, Rev. Geophys., 50, RG2001, doi:10.1029/2011RG000369, 2012.

Tosca, M. G., Randerson, J. T., Zender, C. S., Nelson, D. L., Diner, D. J., and Logan, J. A.: Dynamics of fire plumes and smoke clouds associated with peat and deforestation fires in Indonesia, J. Geophys. Res., 116, D08207,
660   doi:10.1029/2010JD015148, 2011.

Trentmann, J., Luderer, G., Winterrath, T., Fromm, M. D., Servranckx, R., Textor, C., Herzog, M., Graf, H.-F., and Andreae, M. O.: Modeling of biomass smoke injection into the lower stratosphere by a large forest fire (Part I): reference simulation, Atmos. Chem. Phys., 6, 5247–5260, doi:10.5194/acp-6- 5247-2006, 2006.

Tsigaridis, K., Daskalakis, N., Kanakidou, M., Adams, P. J., Artaxo, P., Bahadur, R., Balkanski, Y., Bauer, S. E., Bellouin, N.,
665   Benedetti, A., Bergman, T., Berntsen, T. K., Beukes, J. P., Bian, H., Carslaw, K. S., Chin, M., Curci, G., Diehl, T., Easter, R. C., Ghan, S. J., Gong, S. L., Hodzic, A., Hoyle, C. R., Iversen, T., Jathar, S., Jimenez, J. L., Kaiser, J. W., Kirkevåg, A., Koch, D., Kokkola, H., Lee, Y. H., Lin, G., Liu, X., Luo, G., Ma, X., Mann, G. W., Mihalopoulos, N., Morcrette, J.-J., Müller, J.-F., Myhre, G., Myriokefalitakis, S., Ng, N. L., O'Donnell, D., Penner, J. E., Pozzoli, L., Pringle, K. J., Russell, L. M., Schulz, M., Sciare, J., Seland, Ø., Shindell, D. T., Sillman, S., Skeie, R. B., Spracklen, D., Stavrakou, T., Steenrod, S. D., Takemura,
670   T., Tiitta, P., Tilmes, S., Tost, H., van Noije, T., van Zyl, P. G., von Salzen, K., Yu, F., Wang, Z., Wang, Z., Zaveri, R. A., Zhang, H., Zhang, K., Zhang, Q., and Zhang, X.: The AeroCom evaluation and intercomparison of organic aerosol in global models, Atmos. Chem. Phys., 14, 10845–10895, doi:10.5194/acp-14- 10845-2014, 2014.

Turquety, S., Logan, J. A., Jacob, D. J., Hudman, R. C., Leung, F. Y., Heald, C. L., Yantosca, R. M., Wu, S., Emmons, L. K., Edwards, D. P., and Sachse, G. W.: Inventory of boreal fire emissions for North America in 2004: Importance of peat burning
675   and pyroconvective injection, J. Geophys. Res.-Atmos., 112, D12S03, doi:10.1029/2006JD007281, 2007.

Urbanski, S.: Wildland fire emissions, carbon, and climate: Emission factors, Forest Ecol. Manage., 317, 51–60, doi: 10.1016/j.foreco.2013.05.045, 2014.

Vernon, C. J., Bolt, R., Canty, T., and Kahn, R. A.: The impact of MISR-derived injection height initialization on wild- fire and volcanic plume dispersion in the HYSPLIT model, Atmos. Meas. Tech., 11, 6289–6307, doi:10.5194/amt-11-6289-2018,
680   2018.

Val Martin, M., Logan, J. A., Kahn, R. A., Leung, F. Y., Nelson, D. L., and Diner, D. J.: Smoke injection heights from fires in North America: analysis of 5 years of satellite observations, Atmos. Chem. Phys., 10, 1491–1510, doi: 10.5194/acp-10-1491-2010, 2010.

Val Martin, M., Kahn, R. A., Logan, J. A., Paugam, R., Wooster, M., and Ichoku, C.: Space-based observational constraints
685   for 1- D fire smoke plume-rise models, J. Geophys. Res.-Atmos., 117, doi:10.1029/2012JD018370, 2012.

Val Martin, M., Kahn, R. A., and Tosca, M.: A Global Analysis of Wildfire Smoke Injection Heights Derived from Space-Based Multi-Angle Imaging, Remote Sens., 10, 1609, doi: 10.3390/rs10101609, 2018.

Winker, D. M., Tackett, J. L., Getzewich, B. J., Liu, Z., Vaughan, M. A., and Rogers, R. R.: The global 3-D distribution of tropospheric aerosols as characterized by CALIOP, Atmos. Chem. Phys., 13, 3345–3361, doi:10.5194/acp-13-3345-2013,
690   2013.

Worden, H.M., Deeter, M.N., Edwards, D.P., Gille, J.C., Drummond, J.R., and Nedelec, P.: Observations of near-surface carbon monoxide from space using MOPITT multispectral retrievals, J. Geophys. Res.: Atmos., 115, D18, 27, doi:10.1029/2010JD014242, 2010.

Yu, P. F., Toon, O. B., Bardeen, C. G., Zhu, Y. Q., Rosenlof, K. H., Portmann, R. W., Thornberry, T. D., Gao, R. S., Davis, S.
695   M., Wolf, E. T., Gouw, J., Peterson, D. A., Fromm, M. D., and Robock, A.: Black carbon lofts wildfire smoke high into the stratosphere to form a persistent plume, Science, 365, 587–590, doi: 10.1126/science.aax1748, 2019.

Zhu, L., Martin, M. V., Gatti, L. V., Kahn, R., Hecobian, A., and Fischer, E. V.: Development and implementation of a new biomass burning emissions injection height scheme (BBEIH v1.0) for the GEOS-Chem model (v9-01-01), Geosci. Model

Dev., 11(10): 4103-4116, doi:10.5194/gmd-11-4103-2018, 2018

700   **Figures**
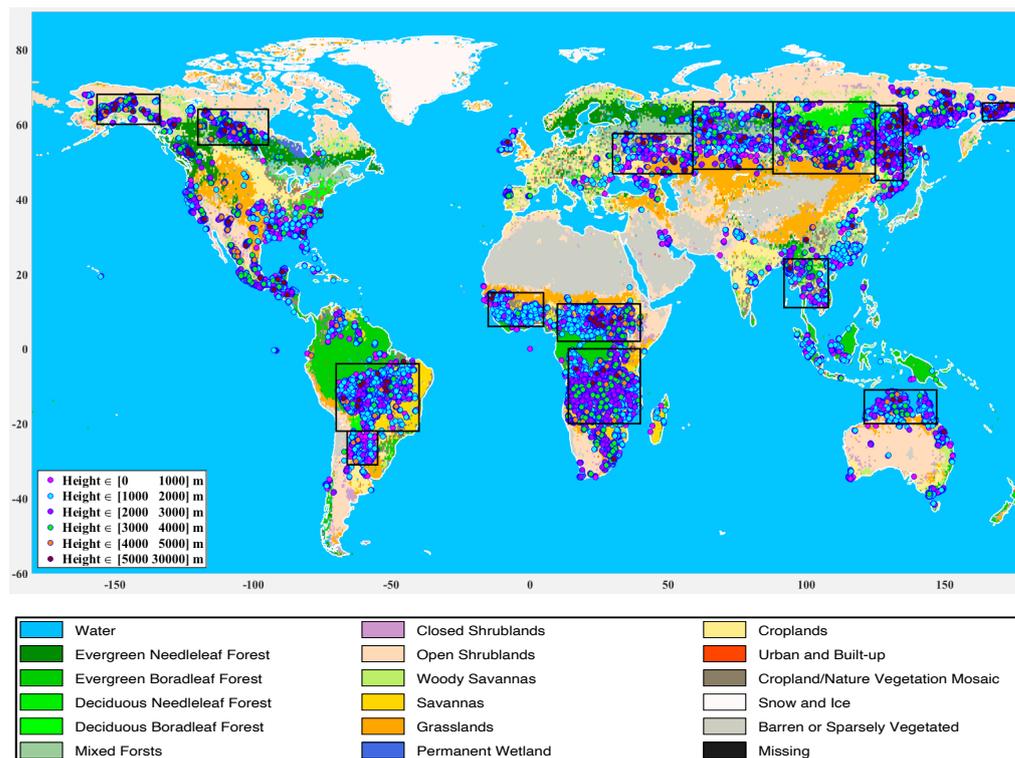
Figure 1: Land surface type at each of the daily MISR measurements from January 2008 to June 2011. Each dot corresponds to an individual aerosol plume.
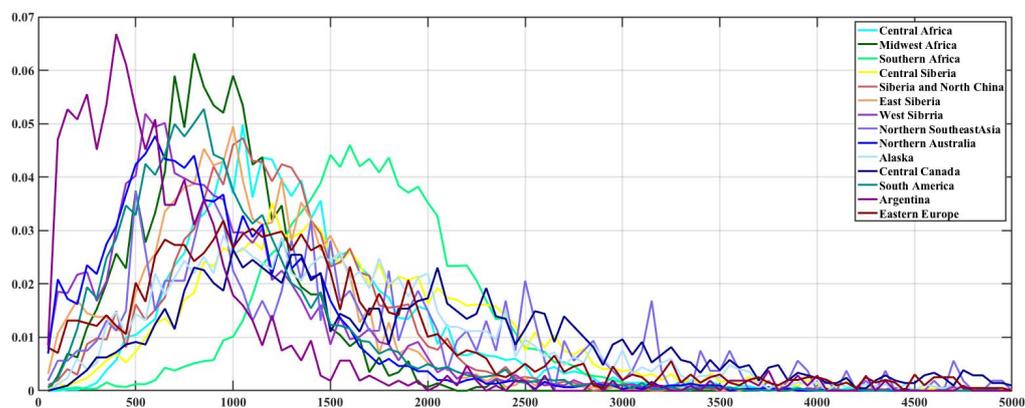
705

Figure 2: PDFs of all daily MISR plume height measurements (which are 5000m or less) over each of the geographic regions, from January 2008 through June 2011.
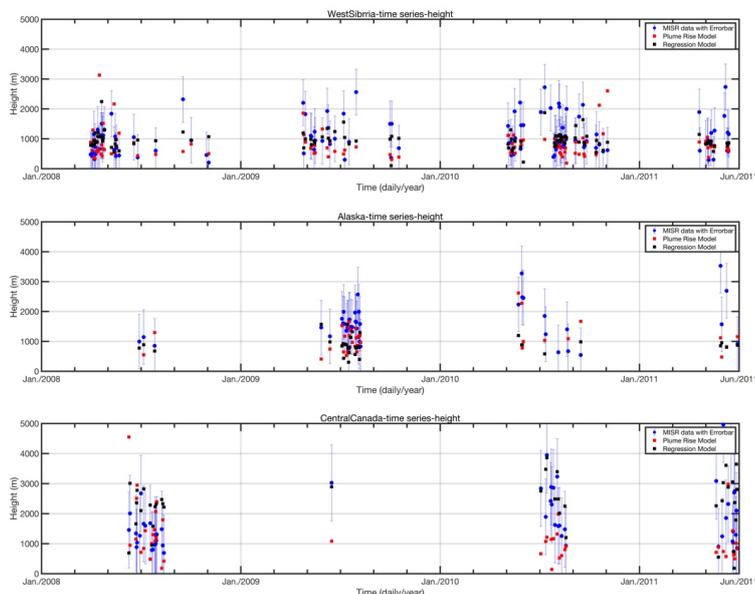
710

Figure 3: Time series of daily average measured MISR aerosol height (circles, m) with an error bar (1 sigma, m); the plume rise model height (red squares, m), and the regression model height (black squares, m), over (a) West Siberia, (b) Alaska, and (c) Central Canada. Missing data points are due to a lack of MISR measurements.

Tables

	C_{NO2} (entire box)	C_{NO2} (fire only)	C_{CO} (entire box)	C_{CO} (fire only)
Central Africa	1.36e+15	3.24e+15	2.24e+18	2.49e+18
Midwest Africa	1.20e+15	3.12e+15	2.45e+18	2.60e+18
Southern Africa	1.40e+15	3.60e+15	1.94e+18	2.24e+18
Central Siberia	8.63e+14	1.11e+15	2.04e+18	2.78e+18
Siberia and Northern China	1.36e+15	1.13e+15	2.31e+18	2.90e+18
Eastern Siberia	4.74e+14	1.50e+15	2.25e+18	2.38e+18
Western Siberia	1.21e+15	1.70e+15	2.20e+18	2.52e+18
Northern Southeast Asia	1.43e+15	2.94e+15	2.58e+18	3.09e+18
Northern Australia	7.53e+14	1.73e+15	1.50e+18	1.73e+18
Alaska	7.63e+14	1.46e+15	2.07e+18	2.12e+18
Central Canada	5.98e+14	1.02e+15	2.13e+18	2.15e+18
South America	1.16e+15	6.36e+15	1.78e+18	3.08e+18
Argentina	1.22e+15	1.32e+15	1.51e+18	1.62e+18
Eastern Europe	1.70e+15	1.81e+15	2.25e+18	2.79e+18

715   **Table 1: Statistical summary of measured column loadings of OMI NO2 [molecule/cm2] and MOPITT CO [molecule/cm2] averaged from January 2008 to June 2011, over each entire boxed region (entire box) as well as the subset in space and time containing active fires (fire only).**

720

Region	α	β	γ	δ	ε	R²
Siberia and North China	110	318	NaN	300	-518	0.26
East Siberia	-163	-657	1480	NaN	437	0.41
West Siberia	241	196	-221	NaN	-263	0.22
Northern Southeast Asia	367	139	912	NaN	355	0.31
Northern Australia	211	-4	NaN	1820	-1580	0.24
Alaska	163	18	2674	-892	NaN	0.37
Central Canada	-232	334	NaN	3190	-1970	0.50
South America	226	57	314	NaN	8	0.30

Table 2: Best fit values for the various coefficients of the regression plume rise height models based on Eq.1-7.

	MISR data	Plume Rise Model	RMS	Regression Model	RMS
Siberia and North China	1.27 *(0.97)*	NAN	NAN	1.07 *(0.30)*	0.42
Eastern Siberia	1.12 *(1.00)*	NAN	NAN	1.32 *(0.65)*	0.35
West Siberia	0.95 *(0.77)*	0.79 *(0.95)*	0.67	0.97 *(0.29)*	0.47
Northern Southeast Asia	1.57 *(1.03)*	NAN	NAN	1.42 *(0.51)*	0.68
Northern Australia	0.90 *(0.62)*	NAN	NAN	1.12 *(0.38)*	0.52
Alaska	1.57 *(0.91)*	1.39 *(3.03)*	0.88	1.26 *(0.45)*	0.77
Central Canada	1.97 *(1.26)*	1.73 *(2.19)*	1.36	2.13 *(1.72)*	1.20
South America	0.97 *(0.66)*	NAN	NAN	0.95 *(0.22)*	0.37
Argentina	0.69 *(0.70)*	0.65 *(0.25)*	0.40	NAN	NAN
Eastern Europe	1.41 *(1.05)*	1.27 *(2.67)*	0.85	NAN	NAN

Table 3: Statistics of measured MISR plume heights and (standard deviations) [2nd column, km] using all daily data from Jan. 2008 to Jun. 2011; the plume rise model results and (standard deviations) [3rd column, km]; RMS between measurement and plume rise model [4th column, km]; the regression model results and (standard deviations) [5th column, km]; and RMS between measurement and regression model [6th column, km]. NaN indicates that the respective model failed over the given region.

725